Neutron-induced ^{235}U fission spectrum measurements using liquid organic scintillation detectors

Andreas Enqvist,* Brian M. Wieger, Lu Huang, Marek Flaska, and Sara A. Pozzi
Department of Nuclear Engineering and Radiological Sciences, University of Michigan, Ann Arbor, Michigan 48109, USA

Robert C. Haight and Hye Young Lee
Los Alamos National Laboratory, Los Alamos, New Mexico 87545, USA

Elaine Kwan and Ching Yen Wu
Lawrence Livermore National Laboratory, Livermore, California 94551, USA
(Received 14 August 2012; published 12 December 2012)

Measurements have been performed at Los Alamos Neutron Science Center to acquire neutron fission spectra of ^{235}U in the energy range between 0.5 and 10 MeV. These new data complement the currently available experimental data, which are not well known in the energy range below 1 and above 5 MeV. Organic liquid scintillation detectors (EJ-309s) were used together with a digital data-acquisition system. The EJ-309 detectors show excellent pulse shape discrimination capabilities and this is vital for identifying only neutron pulses and rejecting γ-ray pulses. The measurement data show the dependence of average fission neutron energy as a function of the inducing neutron energy. The data agree well with previously published measurements and Watt spectra fits for energies up to tens of MeV. At high fission-inducing neutron energies the spectrum deviates from Watt-spectra fits. The increased energy deposited in higher energy neutron-induced fissions does not significantly increase emitted fission neutron energies for up to 10 MeV. A significant decrease in neutron energy around second-chance fission cannot be observed beyond the current measurement uncertainties.

DOI: 10.1103/PhysRevC.86.064605 PACS number(s): 25.85.Ec, 29.25.Dz, 29.30.Hs, 29.40.Mc

I. INTRODUCTION

Knowledge of the neutron fission spectra of common nuclear isotopes is of importance to many fields of nuclear engineering, such as reactor physics and nuclear safety. Most measurements rely on fast-neutron elastic scattering to create signals in the detectors of choice. Such detection systems have the benefit of typically having quick response times; thus they can correctly discriminate one fission event from another. The drawbacks, however, lie in the fact that they have a mediocre detection efficiency, due to difficulties in creating large encompassing detector systems.

In this work liquid scintillation detectors were used. The detection efficiency is reduced for low-energy neutrons, which frequently deposit less energy than the detection threshold (typically 1 MeV or lower). Likewise, the efficiency is lower for measuring high-energy neutrons, whose scattering cross section decreases with increasing energy. These facts, together with some other measurement limitations, have led to fewer experimental data for the fission spectrum being available below 1 and above 5 MeV.

Much work within nuclear materials detection and safeguards is performed using computer simulations with Monte Carlo codes. Those codes rely on accurate measurements or best-estimate models for cross sections for different particles, particle emissions spectra, and other nuclear data. Therefore, measurements that help verify lesser known data or even expand the known region of models and databases are of great importance.

In an attempt to investigate the neutron-energy regions of interest, a measurement system based on liquid scintillation detectors with excellent pulse shape discrimination (PSD) between neutrons and γ rays, digital data-acquisition systems, and analysis algorithms was developed at the University of Michigan (UM) and used at Los Alamos National Laboratory (LANL). The Los Alamos Neutron Science Center (LANSCE) is based on an 800-MeV proton accelerator which creates a pulsed, white neutron source by means of spallation reactions on a tungsten target [1,2]. Through different ports and collimations, an array of neutron beams at various flight paths are created. The Weapons Neutron Research (WNR) beam at 30° right (see Fig. 1) was utilized in this work [1–3].

To measure neutron-induced neutron fission energy spectra, a double time-of-flight (TOF) approach was used [4,5]. First, the incoming neutron energy from the beam is determined from the time difference between spallation emission and fission induced by the neutron. The flight path from the spallation target to a ^{235}U fission chamber (FC) of over 22 m allows for good energy resolution of the fission-inducing neutrons. The time of fission to the time of detection of the fission neutrons is used to determine the energy of the emitted neutrons. That TOF is achieved over an 80-cm flight path between the FC and the detectors, which allows for adequate time and energy characterization of the fission neutrons. As the exact location of interaction in each detector is unknown there is an uncertainty associated with each determined energy in the TOF setup. The neutron interaction in the detectors is dependent only on the well-known scattering cross sections of hydrogen and carbon. Therefore, Monte Carlo simulations of interaction depth and the dependence on neutron energy were conducted. Corrections to the effective TOF distance and interaction

*enqvist@umich.edu

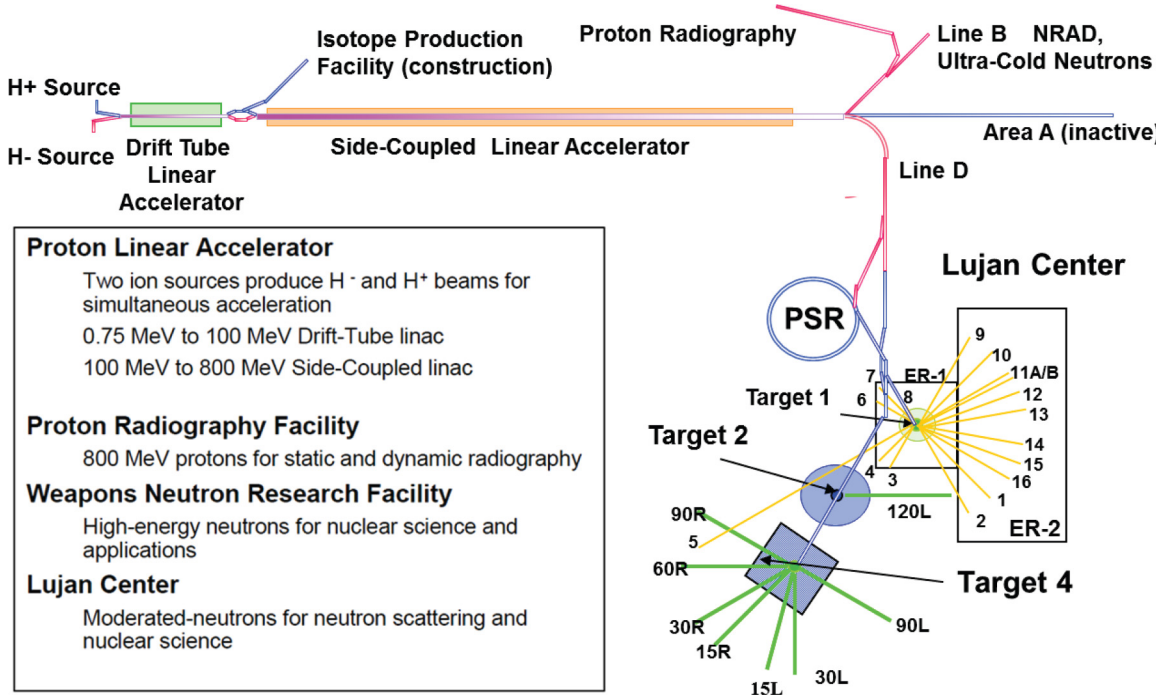

FIG. 1. (Color online) Description of LANSCE facility [2].

times depending on neutron energy were performed. This procedure can reduce the uncertainty by more than a factor of 2 in determination of average energy for the detectors used, which had depths of several mean free paths. This becomes apparent especially for our relatively deep detectors, which would impose a large uncertainty on the flight path, while interaction depth effects from simulations could limit that to 1-σ errors similar to the uncertainties used for statistics and other factors.

II. DESCRIPTION OF THE EXPERIMENTAL SETUP

The measurement was performed in July 2010 during the course of approximately 60 h. The data-acquisition time was initially somewhat limited by the accelerator not operating at full specifications. In addition, the measurement was ended by a power outage caused by lightning.

Five EJ-309 [6] cylindrical liquid scintillation detectors, with a depth of 13.3 cm and a diameter of 13 cm, were used for the measurements. The EJ-309 liquid has a high flash point (144 °C) and low chemical toxicity, while having a short light-emission component of 3.5 ns, which results in excellent timing properties.

The detectors were placed at a distance of 80 cm to the center of the ^{235}U FC (see Fig. 2). The center detector was at a right angle with the neutron beam and the five equally spaced detectors extended to a total angle of approximately 60°. The FC itself was aligned along the incoming neutron beam and can be seen in Fig. 3. Data acquisition was performed utilizing a 250-MHz, 12-bit (∼11-bit effective), eight-channel, CAEN V1720 digitizer. Seven channels were used: the ^{235}U FC, the beam trigger (spallation source), and five EJ-309 detectors.

The FC was chosen as the triggering channel, which heavily reduced the amount of data acquired. The data window was set to 1808 ns, meaning a minor overlap of the accelerator pulse spacing of 1788.8 ns occurred to ensure a trigger could always be identified to determine the energy of the incident neutron that caused the fission. The detectors were calibrated using γ-ray sources to have the same gain and to determine the kiloelectronvolt electron equivalent (keVee) threshold in digitizer units (V).

The LANSCE neutron beam spectrum resembles a Maxwellian distribution with a temperature of approximately

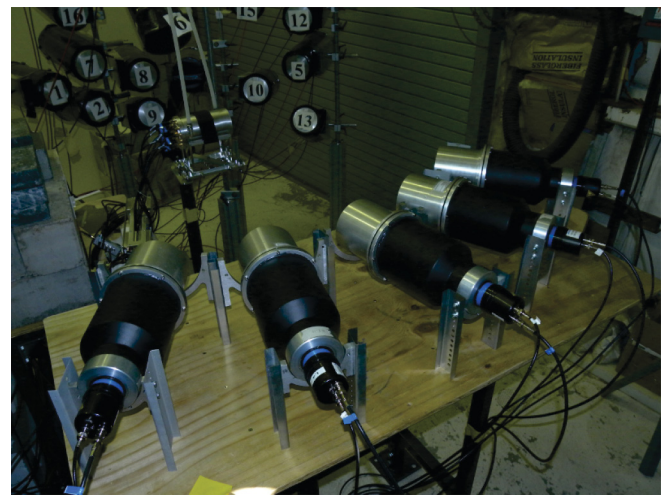

FIG. 2. (Color online) Measurement setup with five EJ-309 liquid scintillation detectors placed 80 cm from the ^{235}U fission chamber. The stationary FIGARO array [4] can be seen with its 20 detectors in the background.

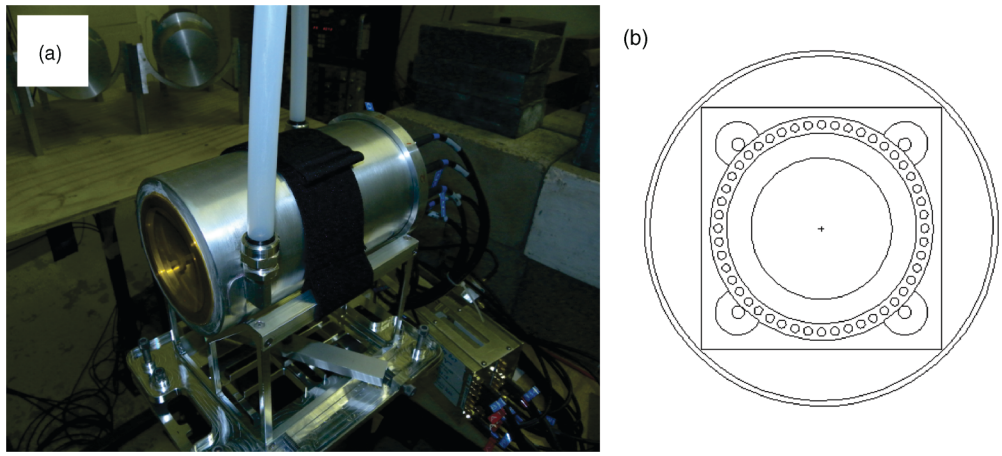

FIG. 3. (Color online) The fission chamber from Lawrence Livermore National Laboratory. (a) The beam enters through a kapton window on the opposite side. (b) A rendering of the modeled fission chamber showing the cross section of the inner structure.

2 MeV and a high-energy tail extending beyond 300 MeV [7]. To reduce the number of γ rays and low-energy neutrons, absorbers of 1.27 cm of CH_2 and 1.27 cm of lead are placed in the beam at approximately 6 m from the source. More detailed flux measurements using fission ionization chambers in the beam are described in Ref. [8].

A parallel-plate avalanche counter (PPAC) made at the Lawrence Livermore National Laboratory is used as a FC at a distance of 22.675 m from the spallation target. The PPAC contains thin foils, ten of which have ^{235}U deposited on each side with a total mass of $\sim$113 mg and a target spot of 4 cm in diameter [9]. The PPAC provides $\sim$1 ns timing resolution when triggering on the fission fragments. There are also α decays in the fissile material, but with the absence of other materials such as oxides there are virtually no α-induced neutrons generated. The α decays do however increase the trigger rate of the FC by approximately 26 triggers per second. This can be compared to the approximately 60 triggers per second observed from neutron-induced fissions when the beam was operational. Most of the α decays in the FC are removed by appropriate threshold. However, to avoid loss of real fission events some α decays will still generate pulses in the fission chamber.

The PPAC contains individual fission plates separated in the direction of the neutron beam path. Although the PPAC has been optimized for detecting the fission events, a small fraction of events can be lost if the fission fragments are emitted at angles parallel to the plate itself. The detectors extend some angle in the perpendicular direction of the fission plates to encompass various angles of the fission fragment fissions. The bias due to undetected fission should be minor due to the high detections efficiency [9], but it cannot be quantified in the current setup with adequate accuracy. The dependence on the fission fragment direction for incoming MeV neutrons has been studied previously [10], with some models being based on the semiclassical conservation of momentum. With the additional departed neutron energy to the fission event only a minor number of events should have very close to 180° opposing fission fragments, thus somewhat alleviating the fission detection deficiency even if one fragment is emitted parallel to the fission plate. Had the detector array extended a full 4π then the directional bias could be removed. Future measurements aim at correcting this deficiency.

A. Reference measurements with ^{252}Cf

Knowing the energy-dependent detection efficiency is of the utmost importance when trying to determine the incoming neutron spectrum on the detectors. Hence, a careful calibration using a TOF measurement with a ^{252}Cf source, with a well-characterized spectrum, was performed in a laboratory environment.

Specifically, inherent time delays in the photomultiplier tubes (PMTs) were characterized using the γ-ray burst from the ^{252}Cf spontaneous fission event. These delays were reverified using the actual LANSCE measurement data. The PMTs used were 5-in. Photonis XP4512B tubes. The EJ-309 detector efficiency strongly depends on the threshold applied. Figure 4 shows the measured detection efficiency. The efficiency can be observed to decline with increasing neutron energy, as a consequence of the reduced neutron scattering cross sections (longer mean free path) at higher energies. The LANSCE measurement and the efficiency measurement used the same setup and threshold (50 keVee, approximately 0.5 MeV neutron energy deposited). The low threshold combined with doing the efficiency measurement with all five detectors present gives a rather high detection efficiency. Since detection of neutrons depends on scattering rather than absorption in these detectors, the neutrons could generate a pulse in an adjacent detector if they have sufficient energy. To quantify this effect, simulations were performed to quantify this crosstalk. The measurement of the efficiency was also done with the same setup used at LANSCE. In this way, the effect of crosstalk generating extra pulses is already included in the efficiency. The difference in average number of neutrons per fission ($\overline{\nu}$) between ^{252}Cf and ^{235}U should only have a minor effect, apart from any bias or uncertainty in $\overline{\nu}$, which is used for normalizing both the efficiency, and later the flux measured at LANSCE.

It is worth noting that the efficiency, while very low, does extend to energies below what can be expected from the threshold in keVee when converted to neutron energy. The

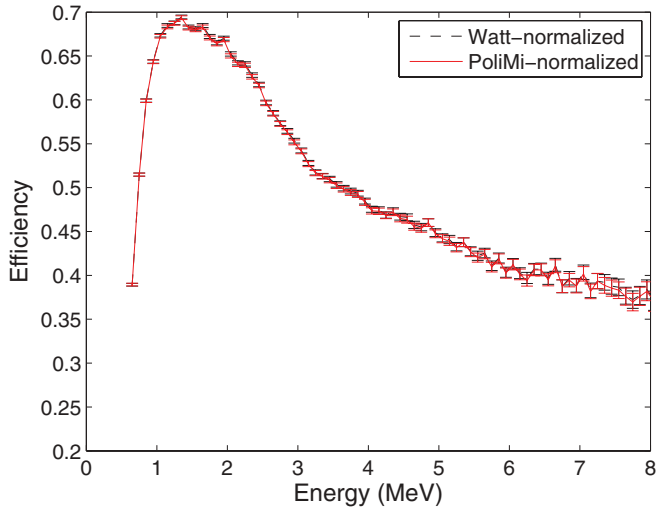

FIG. 4. (Color online) Measured efficiency using two different reference ^{252}Cf spectra, the built-in MCNPX-POLIMI [11] spectrum and one from a Watt curve [$a = 1.18$, $b = 1.034\,19$ in Eq. (1)]. Error bars shown are the 1-σ error related to the statistics of the measurement.

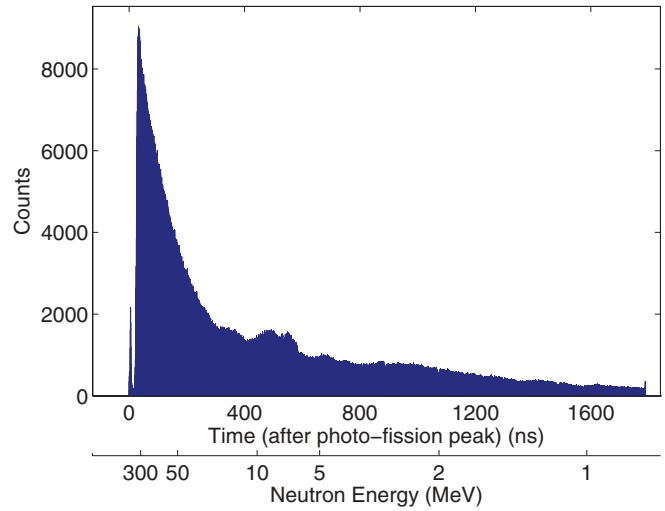

FIG. 5. (Color online) TOF spectrum from the beam to the fission chamber. Time is normalized to the photofission peak, which occurs 75.6 ns after the spallation event with a flight path of 22.675 m.

reason for this is that the resolution of the detector (e.g., fluctuations in light conversion and electron cascades) can bring some pulses up above the threshold when they should otherwise have been too small to be recorded. At low pulse heights the resolution for these detectors approaches 30%. This low-energy range is however not used due to the very small efficiency, which with the correspondingly small counts from the experiment will lead to severely expanded uncertainties. Above 8 MeV neutron energy the measured efficiency also drastically decreases due to the limited dynamic range of the digitizer used (2 V). Thus some pulses are removed because their pulse heights are too high. To avoid this problem the data presented thus only extend up to 8 MeV.

III. MEASUREMENT RESULTS AND DISCUSSION

A. TOF results

The offline data analysis consists of finding at least three correlated triggers in the stored data: beam trigger for the starting time, FC trigger for determining the incident neutron energy and starting time of the fission emission, and finally a pulse trigger in at least one detector confirming detection of a neutron or γ ray.

The signals of the FC and the spallation source (proton beam) were converted with analog constant fraction discriminator modules to provide constant logical waveforms with minimal time variation, leading to a time spread in the pulse shape of less than 0.1 ns between different recorded logical waveforms. With the long flight path the arrival of the logical square pulses from the beam trigger at the data-acquisition system as well as at the FC was strongly delayed. As a result of this and the long time delay from source generation to arrival at the FC for lower energy neutrons ($<$2 MeV), it was common to observe the following beam pulse in the time window set by the fission trigger. The pulsing interval was however very stable and excellent timing was achieved even when timing was done on adjacent beam triggers.

The measured TOF spectrum between the beam and the FC can be observed in Fig. 5. The corresponding energy converted from the travel time to arrival is also indicated in the figure. The photofission peak can be observed at time 0 in the figure. It is generated by high-energy γ rays which are created during the spallation process. Some of those will generate photofissions in the FC, which helps determine absolute signal delays in the setup. The overall number of photofissions is negligible for neutron background, and those events are removed by time cuts.

Figure 6 shows the γ-ray and neutron TOF spectra from the FC to the liquid scintillation detectors. The data show all five detectors added together for better statistics. The time was normalized using the γ-ray flash from fission, which occurs

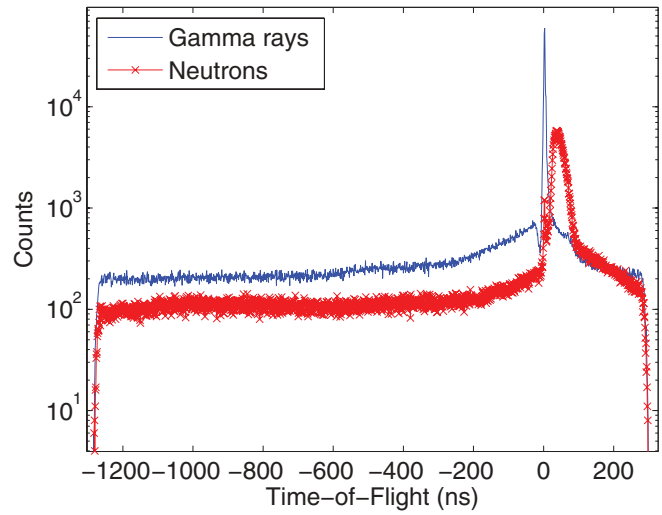

FIG. 6. (Color online) TOF plot showing the time difference between the five EJ-309 detectors and the FC. The γ-ray peak was used to characterize individual signal delays.

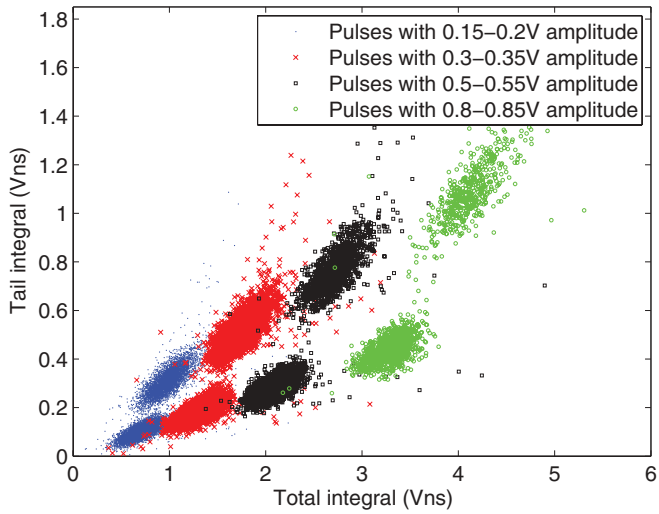

FIG. 7. (Color online) Pulse shape discrimination scatter plot as a function of pulse-height regions. The reduced separation for lower energy pulses is clearly observed.

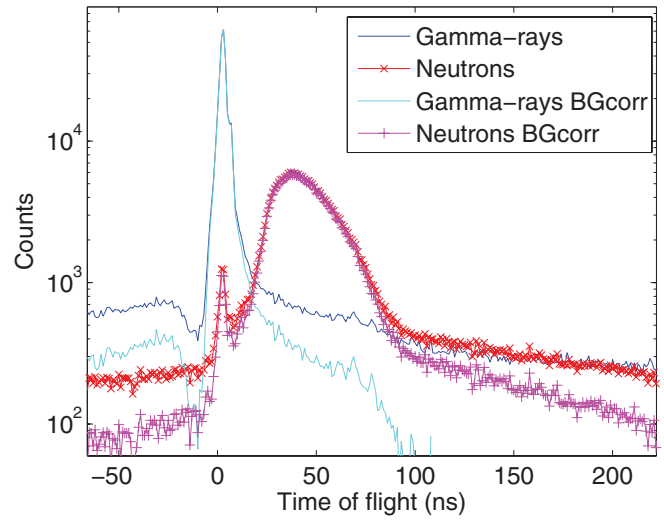

FIG. 8. (Color online) Measured TOF showing the change in the data once the constant portion of the background (accidental triggers) has been corrected for.

just below 3 ns after the fission. The neutron region can clearly be seen as separate in time from the γ-ray flash.

An optimized PSD method was used for the EJ-309 pulses [12]. The PSD of EJ-309 compares well with the most well known PSD scintillator, NE-213 [6]. The nonlinear PSD discrimination line was chosen in accordance with the methodology shown in Ref. [12]. With the amplitude of the pulses being a most significant factor in the performance of the PSD, the threshold was set just above a value where the neutron-γ separation starts to quickly degrade. An illustration of the pulse-height dependence is seen in Fig. 7.

It can be noted that neither the γ-ray nor the neutron background is constant throughout the time range. This is manifested as a rise in counts toward the FC trigger, both before and after the trigger occurs, caused by the pulsed neutron beam also scattering off the material in the FC. Such scattered neutrons, in suitable detectable energy ranges, occur in the same time frame as many of the fission triggers. The long time window leading up to fission was chosen such that it would be optimized to detect the corresponding beam trigger rather than the following beam trigger.

B. Data analysis

The data analysis consisted of a number of different steps which can be categorized as follows: PSD, pulse timing, TOF analysis, background subtraction, and fission-energy-spectrum unfolding.

The background needs to be subtracted for accurate determination of the incoming neutron-induced fission spectrum. Most notably the time-independent background can be removed by investigating the flat background in the TOF spectra at negative TOF times, far away from the fission trigger.

The effect of such background reduction can be seen in Fig. 8. It is apparent that the bulk of the useful data, which for neutrons extends from approximately 30 to 100 ns, is only affected to a small extent, but the background and especially the γ-ray count rate are strongly reduced outside of the fission γ-ray flash. Other sources of background include room return of neutrons and γ rays and delayed emission of γ rays. The background here was subtracted as a flat background. While this background has a large component, especially for the γ rays distributed over time, there is also a time-dependent background. Due to the variation in fission cross section with neutron energy, fissions will occur with a certain distribution compared to the neutron energy distribution from the spallation source. Those neutrons then create a background from scatters in the fission foils and other FC material, as well as scatters further away from our detector setup. Finding this time-dependent component is, however, complicated since applying random FC triggers to detect the detector background does not capture the time dependence of the neutron source. That contribution is addressed in the data analysis by applying pulse-height cuts to remove neutrons of energies inconsistent with the TOF compared to the fission event.

Once a background-cleaned TOF spectrum is obtained, the time spectrum is converted to energy by the relativistic relationship. Each time slice of the neutron peak corresponds to a certain range of energies for the given flight path. There are some variations to that flight path worth mentioning; most notably, the finite depth of the detector puts a certain constraint on the flight path distance. Furthermore, the fission chamber consists of 10 plates, each having ^{235}U deposited on both sides. One time signal came from the fission chamber by summing the signals from the 10 plates. It is therefore unknown which plate generated the fission. However, only small uncertainties in the flight path were introduced by this method.

The arrival times of neutrons were divided into groups corresponding to 100-keV bins for the incoming neutron energy. It is important to note that, due to the reduction in detection efficiency close to the threshold, there are fewer neutrons detected at lower energies. Likewise, at arrival times corresponding to higher energies, we expect to see few counts based on the fact that the high-energy tail of neutron emission

is small above a few MeV. Additionally, the reduced scattering cross section at higher energies reduces the detector efficiency and thus the number of counts.

C. Neutron energy dependence

The counts at each energy are divided by the detector efficiency to obtain the incoming neutron flux. Figure 9 shows this result for two regions of beam energies: up to 10 and above 10 MeV. It can be expected that, as beam neutron energy increases, energy released after fission increases, hardening the neutron fission spectrum. The results originate from data combined from all five detectors. In the case of very high energy fission-inducing neutrons the fission neutrons will be emitted at increasingly forward angles. This might change the statistics between detectors and increase counts in those that are oriented at a forward angle with respect to the incoming beam. The flux is fitted to Watt curves of the form [13]

$$f(E) = ce^{-E/a}\sinh(\sqrt{bE}), \tag{1}$$

where using the following relationship

$$c = \sqrt{\frac{4}{\pi a^3 b}}e^{-ab/4}$$

will normalize it to a probability density function. While the Watt fit of the measured flux (detected neutrons between approximately 0.5 and 8 MeV) from fissions induced by neutrons below 10 MeV is good, there are larger discrepancies shown for the higher energies. The Watt curve should not be expected to capture the high-energy fissions well, especially when extending over a large range of neutron energies. It is expected that the Watt curve will show limitations [14] also at lower energies given that it is a composition of many spectra depending on inducing neutron energy, as well as given the large range of possible fission fragments.

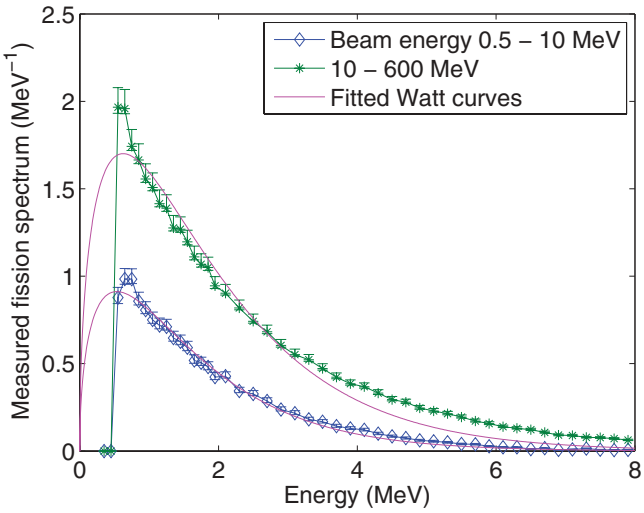

FIG. 9. (Color online) Unfolded spectrum for fissions induced by beam neutrons below or above 10 MeV in energy. Watt spectra, Eq. (1), have been fitted to the experimental data and are shown as solid lines without markers.

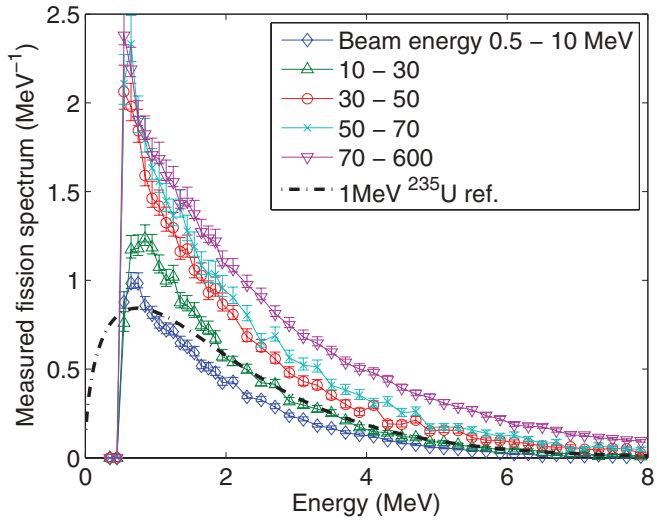

FIG. 10. (Color online) Fission spectra for several high-energy neutron beam ranges. Further dividing the neutron beam energies shows a quickly rising absolute spectra with induced neutron energy. The increasing amplitude corresponds to increases in $\overline{\nu}$. The 1-MeV reference curve is listed in the MCNPX manual and originates from ENDF/B-V [17].

The beam neutrons span a wide range of energies. Using the first TOF the data can be separated into a number of different regions. Figure 10 shows the measured fission spectra for a set of higher neutron ranges. It is clear from the increased amplitude that the average number of neutrons generated ($\overline{\nu}$) increases with fission-neutron energy; this has commonly been shown for lower energy ranges [15,16]. Here it is clearly shown that the trend continues rapidly also beyond 20 MeV.

The measurement was also utilized to investigate the average emitted fission neutron energy at lower fission energies. As can be observed in Fig. 11, the average energy only exhibits minor variation. The data are incomplete due to the lack of detected low-energy neutrons, as well as the removal of some high-energy neutron pulses due to the limited dynamic range of the measurement system. A possible workaround is to calculate the average neutron energy from the fitted Watt spectra. However, statistical fluctuations together with the uncertainty of whether the Watt spectra is an appropriate fit over large variations of inducing neutron energies lead to unsatisfactory results. Calculating the effect of the undetected high- and low-energy neutrons, as well as compensating for the detection efficiency, showed that the overall contributions to the average energy was small when compared to calculating it from the kinematics of the detected fission neutrons. The main contributions to the error bars shown in Fig. 11 come from flight path uncertainties, detector time resolution, and particle misclassification.

Our data exhibit a dip around the energy (∼7 MeV) where second-chance fission becomes possible. The data agree well with previous measurements. The threshold for second-chance fission is above 6 MeV and it has been speculated that the additional pre-scission neutrons would reduce the average neutron energy from such fission events. This has been shown for some isotopes in measurements such as ^{238}U [28], but it

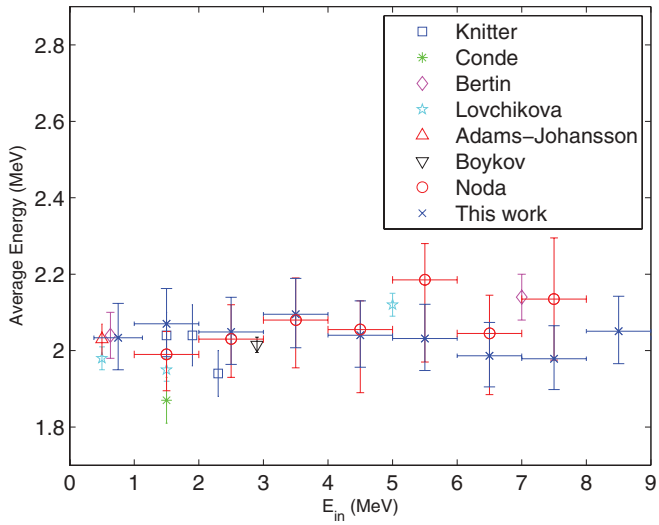

FIG. 11. (Color online) The average emitted neutron energy as a function of the fission-inducing neutron energy. Data are taken from Knitter *et al.* [18], Condé *et al.* [19], Bertin *et al.* [20,21], Lovchikova [22], Adams, Johansson, and co-workers [23–25], Boykov *et al.* [26], and Noda *et al.* [27].

has not been as apparent in measurements of ^{235}U as witnessed in Fig. 11. Our data show a reduction in average energy but the reduction is not large enough compared to the measurement uncertainties to draw any definitive conclusions. The main limitation on the measurement data here is the detector size and setup, while increased statistics can only reduce the error bars by a minor amount. Future data acquisitions using reduced detector depth or possible increased flight path are therefore planned to achieve more conclusive results. Likewise, the data around 15 MeV did not exhibit variations beyond the error bars for any conclusive effect of third-chance fission on average neutron energy.

D. Neutron multiplicities and crosstalk

The crosstalk between the detectors has been accounted for in the detector efficiency; however, it needs to be quantified to determine whether any significant portion of our data is significantly affected by it. The crosstalk quantity was determined by using MCNPX-POLIMI [11] to simulate the experiment and then look at the number of pulses created by crosstalk. From the simulation we find that approximately 1% of all neutron pulses originated from the crosstalk.

Planned future measurements at LANSCE will use a larger detector array of smaller detectors to improve our geometric efficiency and timing and to measure the multiplicity distribution of the fissioning isotope. Table I shows the multiplicity distribution from the current measurement and the contribution of crosstalk to each multiple, again taken from an MCNPX-POLIMI simulation. The crosstalk is defined as the number of coincident pulses where two or more of the pulses were caused by a single neutron. The bottom row of Table I showing the contribution from crosstalk is the amount of crosstalk multiples in relation to the noncrosstalk multiples.

TABLE I. Coincident neutron multiples as detected in the experimental data. The crosstalk percentage is investigated with simulations of the detector setup.

Multiple	*n*	*nn*	*nnn*	*nnnn*
Experimental	533315	8283	100	2
Crosstalk contribution (%)	–	79.06	133.33	–

No crosstalk percentage for the 4*n* multiples was obtained since we did not find any 4*n* multiples in the simulation. A larger number of smaller detectors will allow us to measure higher order multiples while attempting to limit the effect of crosstalk on the data. Using the data from this measurement we can see how large an effect the crosstalk had and what we need to do to improve future measurements.

E. Further discussion on the uncertainties involved

Measurement uncertainties in the form of timing resolution, flight path variations, and PSD errors have been investigated and included in the results. It is noted that the time-dependent background is not removed in this work. Doing so would require very extensive investigations into the fission distribution and scattered beam neutrons. However, much of that contribution was removed by using pulse-height cuts where limitations on maximum pulses in our scintillation detectors were calculated using the measured light generation function of the detectors [29]. The scattered fission neutrons were thoroughly investigated using Monte Carlo simulations, and much of those backgrounds could be removed using background subtraction in combination with constraints on the utilized range of the TOF spectra.

Functional fitting using confidence intervals and uncertainty analysis of the fits was also performed; however, it was found that especially for small beam energy intervals the statistical scatter led to larger uncertainties in the functional fits than what was observed directly in the data. Increased measurement time, or increased detector efficiency by employing more detectors, would likely lead to significant improvements for investigations of the neutron spectrum uncertainty using functional fitting.

Lastly, the PSD performance of the liquids was found to be excellent for larger pulses, while at energies close to the threshold the discrimination between γ-ray and neutron pulses is more complicated. Alternative PSD methods were investigated, and a specific PSD algorithm based of the slow component decay jitter observed in the digitized pulses was developed. The improvement in the misclassification rates was nevertheless low mostly due to already having very good PSD at the used threshold.

IV. MONTE CARLO SIMULATIONS

MCNP-POLIMI is a good tool for investigating time-correlated measurements for neutrons and/or γ rays generated in fissions and other nuclear processes. Recently, the code has been updated to be based off the newer MCNPX code [30]; MCNPX-POLIMI was used for the simulations discussed in this section.

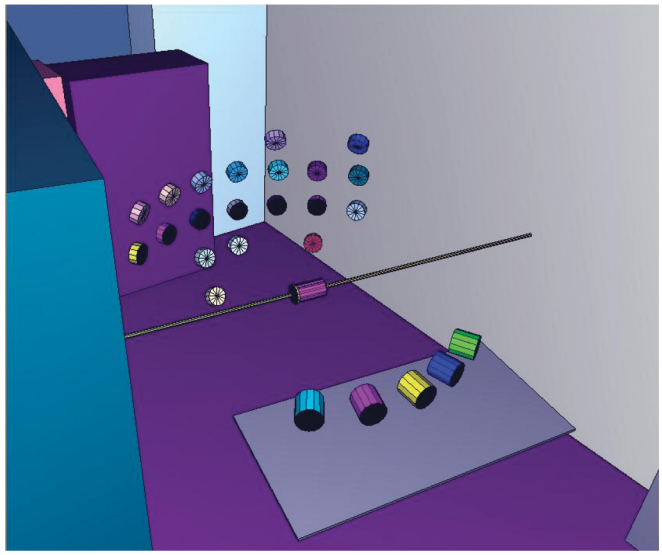

FIG. 12. (Color online) The simulated geometry of the experimental setup at LANSCE. The beam is shown as a bar entering the centrally located fission chamber from the left, before leaving the experimental area to be stopped at a beam stop (not shown).

The geometry (shown in Fig. 12) was investigated to understand the magnitude of the background contributions arising from neutron scatters in the experimental setup. The EJ-309 detectors were modeled with a 97% density of the reported EJ-309 substance to account for the nitrogen bubble occupying 3% of the detector volume. They are shown in Fig. 12 without their housing and PMT; however, those parts were also simulated to investigate whether their modeling is needed. The experimental area and surrounding shielding blocks were modeled following the specifications of the building. The neutron scattering background can be seen in Fig. 13. The measured neutron TOF distribution is shown

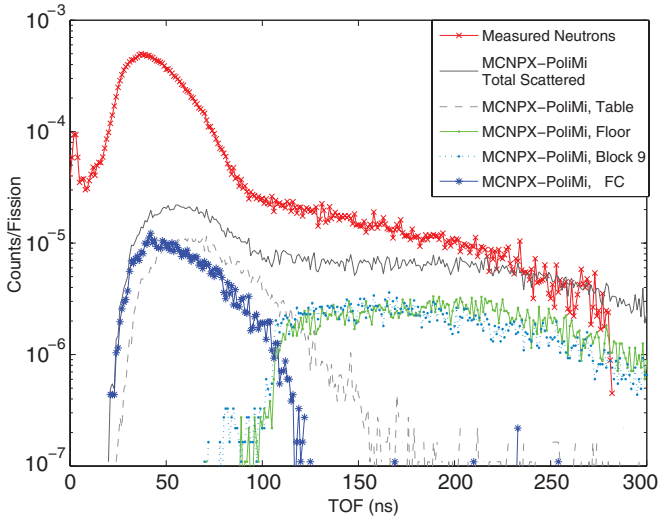

FIG. 13. (Color online) The contributions to the neutron TOF results from neutron scatters in different objects. The table, on which the detectors are placed, is the only notable contribution in the time region of interest.

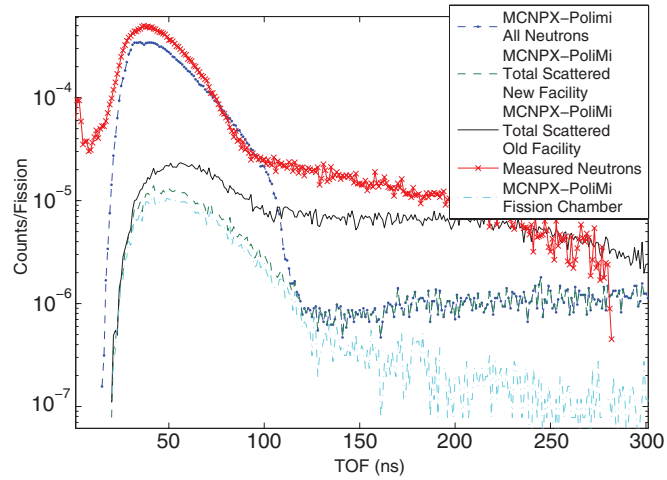

FIG. 14. (Color online) Neutron TOF spectrum including various scatter contributions. The new LANSCE facility under construction will create a one order of magnitude reduction in background counts. This will be especially important for gathering reliable data of fission neutrons below 1 MeV.

together with contributions found in simulations for different components such as table, walls, floor, and FC. It is shown that only the table, on which the detectors were placed, gives notable contributions to the detected neutrons in the TOF region of interest. One can see the long tail extending from approximately 100 to 300 ns after the fission event which is caused by scatters of the emitted fission neutrons in some of the shielding blocks, as well as the floor.

The FC itself also creates in- and out-scatter for the detectors. It was observed in the simulations that the number of neutrons which changed direction such that they created a trigger in the detectors when they originally would not have traveled in the direction of the detectors was almost identical and had the same time distribution as those scattered away from the direction of the detectors. The scatters do, however, reduce the energy of the neutrons, but the scatters were infrequent enough to not have any notable effect on the detected time distribution.

In an attempt to improve the detection capabilities to even lower energies the facility is currently undergoing reconstruction. The main feature of the new experimental area will be an approximately 2-m-deep pit below the measurement area. The simulation results in Fig. 14 show the reduced background, as well as the extended time region, above 100 ns, in which the neutron spectrum clearly separates from the scattered background. Future measurements will take full advantage of the extension into lower neutron energies for improved detection of absolute neutron spectra. The reduction of scattered neutrons by an order of magnitude versus the old setup will further improve also the previously well-defined neutron region by decreasing the uncertainty from background. The contribution from FC scatters can be neglected since it shows a similar temporal distribution as the out-scattered neutrons caused by scatters in the walls of the fission chamber. For future measurements there will also be a contribution coming from scatters in the detector holder itself (but the design is still to be finalized).

Future measurements will also aim at adding additional measurement points in the region below 1 MeV. This is a contested area for measurement data, and additional data here would be of great value. This measurement used a detection threshold such that neutrons down to 0.5 MeV could be detected, but with a heavily reduced efficiency below 1 MeV this creates large uncertainties as the counting statistics is poor. Two adjustments will be made in future measurements to attempt to address this deficiency. One is a reduced detection threshold, which will impair PSD performance but in conjunction with time cuts and pulse-height cuts the data should still offer a significant improvement. The threshold will be chosen suitably low such that postprocessing with various thresholds still lower than previous measurements can be performed with an emphasis on finding a good trade-off between detection efficiency and PSD. The second adjustment will be the additional use of Li-6 enriched glass detectors. These detectors have a resonance, making detection in the few-hundred-keV range possible through neutron capture and possibly elastic scatter depending on the gain used for the detector.

V. SUMMARY AND CONCLUSIONS

It has been demonstrated that liquid scintillation detectors, which detect both γ rays and neutrons, can be favorably used even in high-background environments to measure neutron fission spectra. Specifically, a neutron-induced ^{235}U fission spectrum was measured. The fission spectrum was determined as a function of the incoming energy of the neutron beam at one of the flight paths at LANSCE which generates neutrons in the range from 0.5 MeV up to several hundreds of MeV. Monte Carlo simulations of the whole experimental setup have been performed. In addition, the LANSCE room return was characterized in detail.

The increased energy deposited in higher energy neutron-induced fissions does not create any significant increase in emitted fission neutron energies for the range up to 10 MeV. A decreasing trend is observed around the threshold of the second-chance fission, but no conclusive evidence is seen due to the size of the measurement uncertainties. The ^{235}U neutron fission spectra were also measured as a function of fission-inducing neutron energy. The increase in $\overline{\nu}$ can be clearly observed for increased fission-inducing neutron energies. It is also observed that for high fission-inducing neutron energies a Watt spectrum provides only a coarse description of the flux shape, which cannot capture the high-energy tail of the emitted neutrons.

ACKNOWLEDGMENTS

This work was funded under the Department of Energy, Nuclear Energy University Programs Award No. DE-FG52-10NA29654. The experimental measurements benefited from the use of the LANSCE accelerator facility. The work at Los Alamos was carried out under the auspices of the US Department of Energy at Los Alamos National Laboratory by the Los Alamos National Security, LLC, under Contract No. DE-AC52-06NA25396.

[1] P. W. Lisowski, C. D. Bowman, G. J. Russell, and S. A. Wender, Nucl. Sci. Eng. **106**, 208 (1990).
[2] P. W. Lisowski and K. F. Schoenberg, Nucl. Instrum. Methods Phys. Res., Sect. A **562**, 910 (2006).
[3] H. Condé, R. C. Haight, H. Klein, and P. W. Lisowski, in *Proceedings of the International Conference on Nuclear Data for Science and Technology, Jülich 13–17 May*, edited by S. M. Qaim (Springer-Verlag, Berlin, 1992) p. 386.
[4] R. C. Haight, J. M. O'Donnell, L. Zanini, M. Devlin, and D. Rochman, *Proceedings of the Eleventh International Symposium on Capture Gamma-Ray Spectroscopy and Related Topics*, edited by J. Kvasil, P. Cejnar, and M. Krticka (World Scientific Publishing Co., Singapore, 2003), pp. 451–459.
[5] D. Rochman, R. C. Haight, J. M. O'Donnell, M. Devlin, T. Ethvignot, and T. Granier, Nucl. Instrum. Methods Phys. Res., Sect. A **523**, 102 (2004).
[6] http://www.eljentechnology.com/images/stories/Data_Sheets/Liquid_Scintillators/EJ309%20data%20sheet.pdf, Eljen Technology, P.O. Box 870, Sweetwater, TX 79556.
[7] LANSCE website, http://www.lansce.lanl.gov
[8] S. A. Wender, S. Balestrini, A. Brown, R. C. Haight, C. M. Laymon, T. M. Lee, P. W. Lisowski, W. McCorkle, R. O. Nelson, W. Parker, and N. W. Hill, Nucl. Instrum. Methods Phys. Res., Sect. A **336**, 226 (1993).
[9] C. Y. Wu, R. Henderson, J. Gostic, R. C. Haight, and H. Y. Lee, Technical Report No. LLNL-TR-461044, 2010.
[10] J. E. Simmons and R. L. Henkel, Phys. Rev. **120**, 198 (1960).
[11] S. A. Pozzi, S. D. Clarke, W. J. Walsh, E. C. Miller, J. L. Dolan, M. Flaska, B. M. Wieger, A. Enqvist, E. Padovani, J. K. Mattingly, D. L. Chichester, and P. Peerani, Nucl. Instrum. Methods Phys. Res., Sect. A **694**, 119 (2012).
[12] M. Flaska and S. A. Pozzi, Nucl. Instrum. Methods Phys. Res., Sect. A **577**, 654 (2007).
[13] T. Ethvignot, M. Devlin, R. Drosg, T. Granier, R. Haight, B. Morillon, R. Nelson, J. O'Donnell, and D. Rochman, Phys. Lett. B **575**, 221 (2003).
[14] C. Wagemans, *The Nuclear Fission Process* (CRC Press, Boca Raton, FL, 1991).
[15] D. S. Mather, P. Fieldhouse, and A. Moat, Phys. Rev. **133**, B1403 (1964).
[16] R. J. Howerton, Nucl. Sci. Eng. **62**, 438 (1977).
[17] D. Kinsey, ENDF/B Summary Documentation, Technical Report No. BNL-NCS-17541, 1979.
[18] H. H. Knitter, M. M. Islam, and M. Coppola, Z. Phys. A **257**, 108 (1972).
[19] H. Condé and G. During, Ark. Fys. **29**, 313 (1965).
[20] A. Bertin, R. Bois, and J. Fréhaut, Trans. Am. Nucl. Soc. **22**, 661 (1975).
[21] A. Bertin, R. Bois, and J. Fréhaut, Commissariat à l'Énergie Atomique, Centre d'Études de Bruyères-le-Châtel Report No. CEA-R-4913, 1978 (unpublished).

[22] G. N. Lovchikova and A. M. Trufanov, Vop. At. Nauki Tekhn., Ser.: Yad. Konstanty **1996**, 102 (1996).
[23] J. M. Adams, UK Atomic Energy Authority Report No. AERE-R-8636, 1977 (unpublished).
[24] P. I. Johansson, B. Holmqvist, T. Wiedling, and L. Jeki, US National Bureau of Standards Special Publication No. 425, 1975 (unpublished).
[25] P. I. Johansson and B. Holmqvist, Nucl. Sci. Eng. **62**, 695 (1977).
[26] G. S. Boykov, V. D. Dmitriev, G. A. Kudyaev, Y. B. Ostapenko, M. I. Svirin, and G. N. Smirenkin, Yad. Fiz. **53**, 628 (1991).
[27] S. Noda *et al.*, Phys. Rev. C **83**, 034604 (2011).
[28] T. Ethvignot, M. Devlin, H. Duarte, T. Granier, R. C. Haight, B. Morillon, R. O. Nelson, J. M. O'Donnell, and D. Rochman, Phys. Rev. Lett. **94**, 052701 (2005).
[29] A. Enqvist, C. C. Lawrence, T. N. Massey, and S. A. Pozzi, in *INMM 53rd Annual Meeting Proceedings*, edited by Patricia Sullivan (Institute of Nuclear Materials Management, Deerfield, IL, USA, 2012).
[30] D. P. Pelowitz, MCNPX Users Manual Version 2.7.0, Technical Report No. LA-CP-11-00438, 2011.